

Sonochemical preparation and characterization of nanosized amorphous Co–Ni alloy powders

Kurikka V. P. M. Shafi,^a Aharon Gedanken^{*a} and Ruslan Prozorov^b

^aDepartment of Chemistry, Bar-Ilan University, Ramat-Gan 52900, Israel

^bDepartment of Physics, Bar-Ilan University, Ramat-Gan 52900, Israel

Nanosized amorphous alloy powders of $\text{Co}_{20}\text{Ni}_{80}$ and $\text{Co}_{50}\text{Ni}_{50}$ have been prepared by sonochemical decomposition of solutions of volatile organic precursors, $\text{Co}(\text{NO})(\text{CO})_3$ and $\text{Ni}(\text{CO})_4$ in decalin, under an argon pressure of 100 to 150 kPa, at 273 K. The amorphous nature of these particles was confirmed by various techniques, such as SEM, TEM, SAED, and XRD. A transmission electron micrograph of the heated $\text{Co}_{20}\text{Ni}_{80}$ sample showed near uniform particles with sizes less than 10 nm. Magnetic measurements indicated that the as-prepared amorphous CoNi alloy particles were superparamagnetic. The observed magnetization, measured up to a field of 15 kG, of the annealed $\text{Co}_{20}\text{Ni}_{80}$ sample (54 emu g^{-1}) was significantly lower than that for the reported multidomain bulk particles (75 emu g^{-1}), reflecting the ultrafine nature of our sample. Thermogravimetric measurements of $\text{Co}_{20}\text{Ni}_{80}$ with a permanent magnet yielded a glass transition temperature of 338°C for the amorphous form, and a Curie temperature of 565°C for the crystallized form. The differential scanning calorimetry showed crystallization temperatures of 400°C for $\text{Co}_{20}\text{Ni}_{80}$ and 365°C for $\text{Co}_{50}\text{Ni}_{50}$ amorphous samples.

Amorphous alloys—metallic glasses or glassy metals obtained by rapid quenching of the melt—lack the long range atomic order of their crystalline counterparts. Unlike conventional glasses, which are basically molecular glasses consisting of long chains or networks of covalently bonded atoms, amorphous alloys are essentially atomic glasses in which each atom constitutes a structural unit. Because of their unique electronic, magnetic, and corrosion-resistant properties,^{1–4} they are of technological importance. Ferromagnetic amorphous alloys containing Fe and Co have excellent soft magnetic properties equivalent or superior to those of conventional materials. Some uses include magnetic storage media and power transformer cores.⁵ Resistivities of the amorphous alloys are generally 2 to 4 times larger than the corresponding transition metal crystalline alloys without the glass formers. This results in a smaller eddy current contribution to the permeability and losses, which is very important at higher frequency device applications.⁶

In the past few years, there has been a literary explosion of both theoretical and experimental results on amorphous magnetic alloys. Many series of alloys have now been reported as composed of transition metal alloys with a wide variety of metalloids such as transition metal–metalloid alloys (TM–M) and rare earth–transition metal (RE–TM) alloys. The TM–M alloys typically contain about 80 atom% Fe, Co, Ni with remainder being B, C, Si, P or Al as glass formers. The presence of metalloids lowers the melting point making it possible to quench the alloy through its glass transition temperature rapidly enough to form the amorphous phase. Once produced, the same metalloids stabilize the amorphous phase, but their presence drastically alters the magnetic properties of the alloys. The change in magnetic properties is due to the change in the electronic environment brought about by donating electrons to the d-band and thus lowering the saturation magnetization (M_s) and Curie temperature (T_c). Among the TM–M systems, the Co–Ni alloy system has been least explored, and most of the studies have focused on the Fe–Ni or Fe–Co systems. The Co–Ni alloy system is important since its zero magnetocrystalline anisotropy composition, $\text{Co}_{20}\text{Ni}_{80}$, makes this alloy system potentially important, especially as a magneto-strictive trans-

ducer material.⁷ As in pure Co, the hexagonal close-packed \leftrightarrow face-centred cubic (hcp \leftrightarrow fcc) martensitic phase transformation has likewise been observed in the Co–Ni alloy system.^{8,9} In pure cobalt, the mean transformation temperature is ca. 420°C , which can be reduced to room temperature by the addition of 32% Ni. The interesting feature of the Co–Ni system is its structural evolution, which is exhibited in its reverse transformation (fcc \leftrightarrow hcp) on cooling. The Co–32% Ni shows the reverse transformation at about 120 K on cooling.⁹ Blanco *et al.*¹⁰ have prepared metallic glass ribbons of the alloy system $(\text{Co}_{1-x}\text{Ni}_x)_{75}\text{Si}_{15}\text{B}_{10}$ ($x=0, 0.08, 0.15, 0.22$) by the roller quenching method. They found that Curie temperatures of the samples were less than room temperature for the values of x higher than 0.22. Amamou¹¹ has prepared amorphous alloy foils of $(\text{Co}_x\text{Ni}_{1-x})_{0.78}\text{P}_{0.14}\text{B}_{0.08}$ ($0 \leq x \leq 1$) by the rapid quenching method, using the piston-anvil technique. In another study, Gyorgy *et al.*¹² have reported the variation of room temperature saturation magnetization and Curie temperature in the alloy system $(\text{Co}_{1-x}\text{Ni}_x)_{0.75}\text{P}_{0.16}\text{B}_{0.06}\text{Al}_{0.03}$, as a function of the composition of transition metals. Quasi-binary Ni–Co–B amorphous/crystalloid multilayer films of Ni–Co–B have also been prepared by the electrodeposition method.¹³

To our knowledge, no amorphous Co–Ni binary alloy system without any glass former (metalloid) has been reported, so far, in the literature. Recently, Uzawa *et al.*¹⁴ have reported the preparation of ultrafine crystalline alloy particles of Fe–Ni, Fe–Co, and Co–Ni systems by leaching amorphous Al–Ni–Fe–Ce, Al–Co–Fe–Ce, and Al–Ni–Co–Ce ribbons prepared by melt spinning. Submicron-sized crystalline Co–Ni powders were prepared by precipitation in liquid polyols from cobalt and nickel mixed hydroxides.¹⁵ Here, we discuss the sonochemical synthesis and characterization of nanosized amorphous Co–Ni particles.

Acoustic cavitation (the formation, growth, and subsequent implosive collapse of a bubble in an ultrasonically irradiated liquid) generates a transient localized hot spot with an effective temperature of 5000 K and a sub-microsecond collapse time.^{16–18} The rapid cavitation cooling rate ($> 10^9 \text{ K s}^{-1}$) is much higher than that obtained by the conventional melt-spinning¹⁹ (10^5 to 10^6 K s^{-1}) technique used to prepare amorphous materials.

The foremost criterion for achieving a good sonochemical yield is that the precursor should be volatile, because the

* E-mail: gedanken@ashur.cc.biu.ac.il

primary sonochemical reaction site is the vapor inside the cavitation bubbles.²⁰ Second, the solvent vapor pressure should be lower at the sonochemical temperature, since solvent vapor inside the bubble reduces the collapse efficiency. Suslick *et al.* have employed this new sonochemical method for the preparation of nanosized amorphous powders of Fe, Co, and their alloys,^{21–23} as well as metal carbide Mo₂C.²⁴

We have reported the preparation of amorphous Ni powder by sonochemical decomposition of nickel tetracarbonyl (Ni(CO)₄) as neat liquid or solution in decalin (decahydronaphthalene).²⁵ By varying the precursor, iron pentacarbonyl (Fe(CO)₅), we were able to control the particle size of amorphous Fe.²⁶ Nanosized amorphous powders of γ -Fe₂O₃,²⁷ NiFe₂O₄²⁸ and Fe-Ni alloy²⁹ were also prepared by the sonochemical method.

Experimental

The precursor, cobalt nitrosyl tricarbonyl, was prepared by the usual method. Nickel tetracarbonyl was distilled before use. Nickel tetracarbonyl is a highly poisonous liquid with a high vapor pressure. It is very sensitive to air and moisture, so care should be taken in handling it. Pentane and decalin were dried with sodium metal or a no. 4 molecular sieve and stored in a glove box. The precursor solution was degassed by purging with high purity argon (<10 ppm O₂) prior to sonication.

Co-Ni alloy was prepared by ultrasonic irradiation of a 0.25 M solution of Co(NO)(CO)₃ and Ni(CO)₄ in decalin at 273 K, under 100 to 150 kPa (1 to 1.5 atm) argon, with a high intensity ultrasonic probe (Sonics and Materials, Model VC-600, 1.25 cm Ti horn, 20 kHz, 100 W cm⁻²). After 3 h irradiation, a black powder was obtained, which was centrifuged and washed with dry pentane in a glove box. Centrifuging and washing were repeated at least five times, and the product was then dried under vacuum. The two compositions of Co-Ni (Co₂₀Ni₈₀ and Co₅₀Ni₅₀) were prepared by varying the concentration of the precursors in solution. Amorphous cobalt and nickel were also prepared by following the same method and conditions.

Powder X-ray diffractograms were recorded on a Rigaku X-ray diffractometer (Cu-K α radiation, $\lambda = 0.15418$ nm). Scanning electron micrographs and energy dispersive X-ray analysis (EDX) were carried out on a JEOL JSM-840 electron microscope. Transmission electron micrographs were obtained with a JEOL JEM100SX electron microscope. Magnetization loops were measured at room temperature, using an Oxford Instruments vibrating sample magnetometer. Surface areas (BET method) were measured on a Micromeritics Gemini surface area analyzer. Magnetic force measurements were carried out on a Mettler TGA4000 with a small permanent magnet. Differential scanning calorimetry (DSC) thermograms were obtained on a Mettler-Toledo DSC 25 calorimeter at a heating rate of 10 °C min⁻¹ under flowing pure argon (50 ml min⁻¹). Elemental analyses were carried out on EA 1110 CHNS-O analyzer. All sample preparations and transfers for these measurements were done inside the glove box.

Results and Discussion

We have noticed that the sonochemical efficiency for decomposition is less for Co(NO)(CO)₃ than for Ni(CO)₄, so it is necessary to use an initial excess of Co(NO)(CO)₃ to obtain the required alloy composition. Earlier, for the preparation of Fe-Ni alloys,²⁹ we have observed the same phenomenon, and there we had to use an initial excess of Fe(CO)₅. The poor reactivity of Co(NO)(CO)₃ can be traced to its lower vapour pressure when compared to Ni(CO)₄. As the precursor's vapor pressure increases, its concentration in the bubble (*i.e.* the gas

phase within the collapsing cavity) increases linearly, thus increasing the observed sonochemical reaction rate.

Alloy compositions were determined by elemental and EDX analyses. The EDX profiles of Co₂₀Ni₈₀ and Co₅₀Ni₅₀ are shown in Fig. 1 and 2. Since the atomic numbers of Ni and Co are similar, the ratio of the X-ray intensities from these elements approximates the alloy composition. Since the <10 nm size of these particles is much smaller than is the 100 nm free path for X-ray transmission through solids, the X-ray intensities need not be corrected for absorption and fluorescence effects.

The elemental analyses of the as-prepared samples show that the amorphous alloy powders have over 95% metal by mass, with small amounts of carbon (<3%) and oxygen (<2%). The presence of carbon and oxygen is presumably a result of the decomposition of alkane solvents or adsorbed CO during ultrasonication. The IR spectra of the as-prepared samples showed peaks at 2100 cm⁻¹ characteristic of adsorbed CO molecules on the surface. These adsorbed impurities probably play an important role in stabilizing the amorphous structure of the samples.²⁹ The elemental analyses of the annealed samples (heated at 300 °C under high-purity Ar for 10 h) showed only <0.5% of C, H and O, individually, and this indicated that the adsorbed surface impurities were almost completely removed. The presence of small amounts of C and O could be anticipated from the formation of metal carbides and oxides, during sonication or heating processes. Adsorbed carbonyls on amorphous metals can lead to metal carbides. Suslick *et al.* had reported the formation of Mo₂C

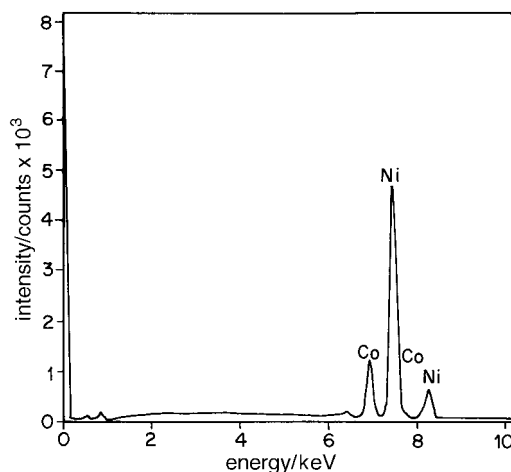


Fig. 1 EDX profile for amorphous Co₂₀Ni₈₀

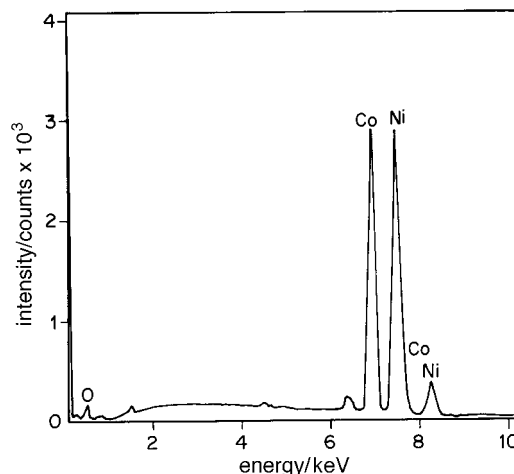


Fig. 2 EDX profile for amorphous Co₅₀Ni₅₀

from adsorbed carbonyl on molybdenum on heating.²⁴ These impurity phases are far less than the detectable level of XRD.

The amorphous nature of the alloy particles was confirmed by various techniques, including SEM, TEM, electron microdiffraction, and X-ray diffraction. A scanning electron micrograph of alloy powder shows coral-like features typical for non-crystalline materials. The TEM images of the as-prepared and heated samples of $\text{Co}_{20}\text{Ni}_{80}$ are shown in Fig. 3. Fig. 3(a) shows no evidence of crystallite formation and indicates that the alloy powders are agglomerates of small particles with overall diameters < 10 nm. Most of the particles are aggregated in a sponge-like form, so it is difficult to determine the particle size exactly. The TEM microdiffraction pattern (inset) of the alloy particles shows only diffuse rings characteristic of amorphous materials. However, a TEM image of the heated specimen [Fig. 3(b)] clearly shows near uniform particles with sizes less than 10 nm. The ED pattern (inset) indicates that these particles are nanocrystalline. The X-ray diffraction pattern for amorphous $\text{Co}_{20}\text{Ni}_{80}$, as well as the heated (at 450 °C for 5 h under argon) samples of α -Co, γ -Ni, $\text{Co}_{20}\text{Ni}_{80}$, and $\text{Co}_{50}\text{Ni}_{50}$ are depicted in Fig. 4. The X-ray diffractogram of the amorphous solid [Fig. 4(a)] shows a broad peak centered around a 2θ value of 44.6°. No sharp diffraction patterns characteristic of crystalline phases appear. After heat treatment under pure argon (< 10 ppm O_2) at 450 °C for 5 h, to induce crystallization, lines characteristic of Co–Ni (fcc) appear. The lack of any feature at 2θ values of 41.72 and 47.60° ($\lambda = 0.15418$ nm), which are the observed positions [see Fig. 4(b)] of crystalline cobalt, hcp α -Co (10.0) and (10.1), respectively, confirms that the Co and Ni become alloyed, rather than forming separate grains. Even for the higher concentration of Co in $\text{Co}_{50}\text{Ni}_{50}$, the phase is still fcc and not hcp. This is in accordance with the reported equilibrium structural phase diagram of Co–Ni binary alloys.³⁰

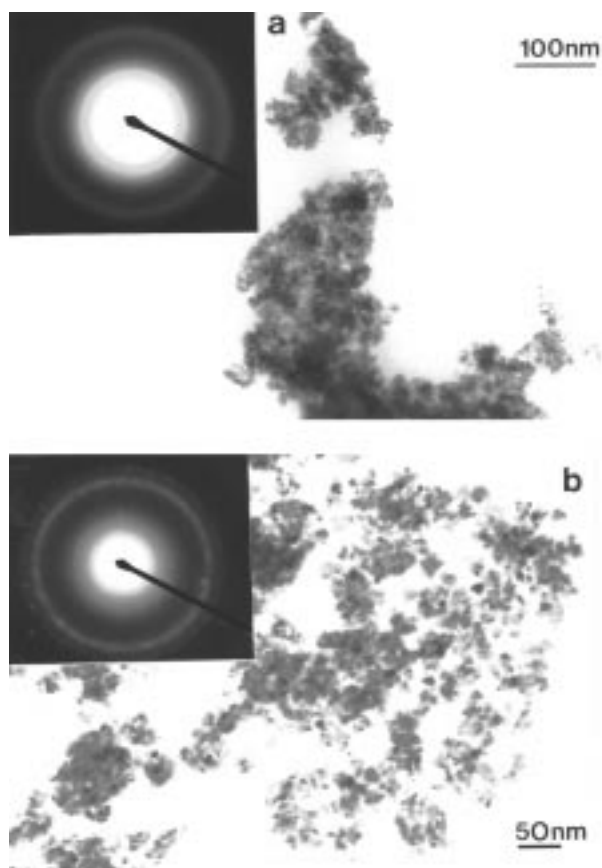


Fig. 3 TEM images of $\text{Co}_{20}\text{Ni}_{80}$ sample with micro-diffraction pattern (inset): (a) as-prepared amorphous, (b) crystalline (heated at 450 °C for 5 h)

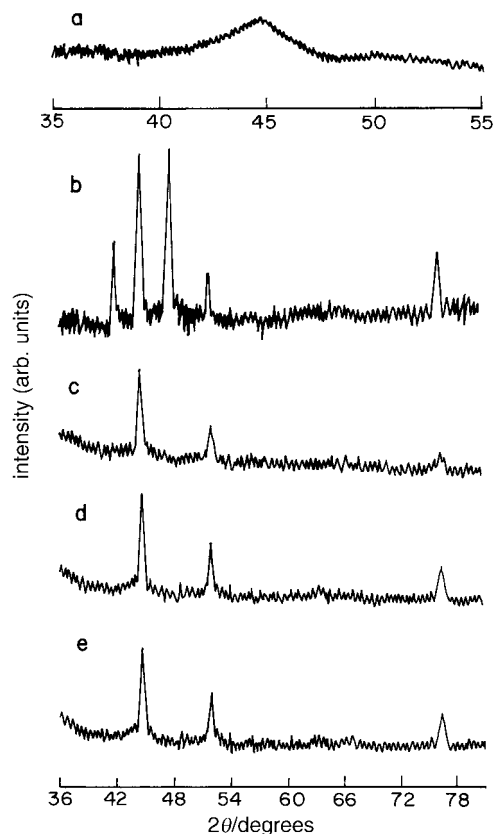


Fig. 4 XRD patterns for: (a) amorphous $\text{Co}_{20}\text{Ni}_{80}$, (b) crystalline α -Co, (c) crystalline $\text{Co}_{20}\text{Ni}_{80}$, (d) crystalline $\text{Co}_{50}\text{Ni}_{50}$, (e) crystalline γ -Ni

Room temperature magnetization curves of the as-prepared amorphous samples of $\text{Co}_{20}\text{Ni}_{80}$ and $\text{Co}_{50}\text{Ni}_{50}$ are shown in Fig. 5. The curve of the amorphous samples does not reach saturation even at a magnetic field of 15 kG, and no hysteresis is found, indicating that the as-prepared (amorphous) Co–Ni particles are superparamagnetic. The magnetization (M) vs. field (H) curve is not found to be pure Langevin type owing to the distribution of particle sizes and the randomly oriented anisotropy axes. Fig. 6 shows the magnetization curves of the annealed samples of $\text{Co}_{20}\text{Ni}_{80}$ heated for 5 h at 300 and 450 °C, respectively. The observed values of magnetization of the annealed samples, 11 and 54 emu g^{-1} (for heating at 300 and 450 °C, respectively), at a high field of 15 kG, are significantly lower than that for the reported¹⁵ multidomain micrometer-sized Co–Ni powder (75 emu g^{-1}), and this reflects the ultrafine nature of our sample. The BET surface areas of the amorphous

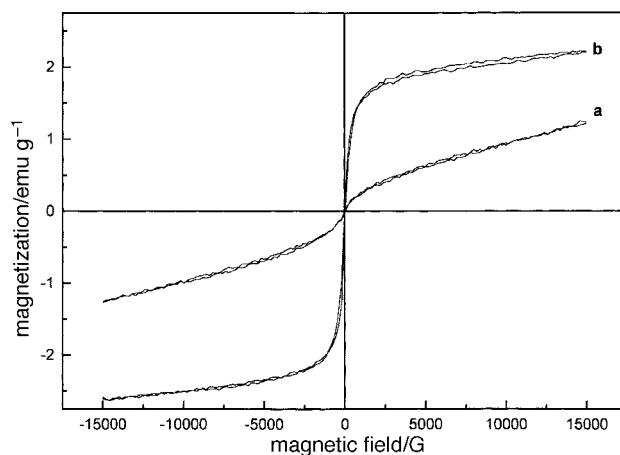


Fig. 5 Room temperature magnetization curves of: (a) amorphous $\text{Co}_{20}\text{Ni}_{80}$, (b) amorphous $\text{Co}_{50}\text{Ni}_{50}$

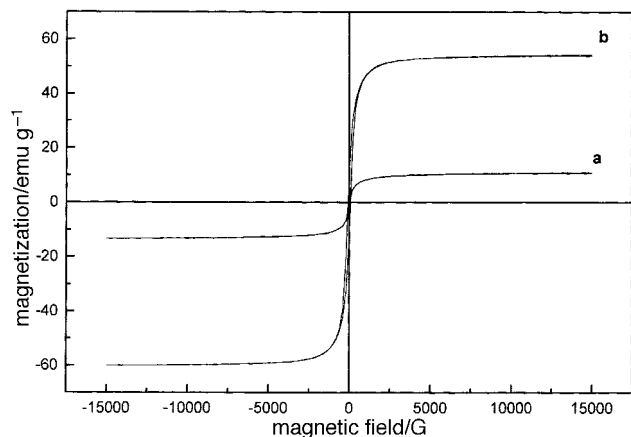


Fig. 6 Room temperature magnetization curves of amorphous $\text{Co}_{20}\text{Ni}_{80}$: (a) heat-treated at $300\text{ }^{\circ}\text{C}$ for 5 h, (b) heat-treated at $450\text{ }^{\circ}\text{C}$ for 5 h

and the heated samples of Co, Ni and Co–Ni alloys are given in Table 1. The decrease in the surface area of the heated sample is due to the increase in particle size because of sintering that occurs on heating. Specifically, the difference in the magnetization value between micrometer-sized and our nano-sized materials can be attributed to the small particle size effect. It is known that magnetic properties, like saturation magnetization and magnetic hyperfine field value, of nanoparticles are much smaller than those of the corresponding bulk materials.^{28,29,31,32} The energy of a magnetic particle in an external field is proportional to its size or volume *via* the number of magnetic molecules in a single magnetic domain. When this energy becomes comparable to kT , thermal fluctuations will significantly reduce the total magnetic moment at a given field. On the other hand, the difference in magnetization for the two samples annealed at 300 and 450 °C can be attributed to the following effects. (a) Increase of the particle size for the sample annealed at 450 °C. This can be readily shown by the decrease in the surface area of the sample compared to the one annealed at 300 °C. (b) Crystalline nature of the sample annealed at 450 °C. The XRD of the samples annealed at 300 °C, shown in Fig. 7, does not show well defined peaks characteristic of crystalline material. It is known that the magnetization of the crystalline materials is larger than that of the amorphous material. The disordered spins in the amorphous system lead to a dispersion in the exchange constant which can suppress the magnetic moment. (c) The large surface area to volume ratio for small particles. The magnetic molecules on the surface lack complete coordination and also the spins are disordered. (d) The small impurities of metal oxides and carbides can also decrease the total magnetization.

Fig. 8(a) shows the result of a magnetic force measurement, obtained with a thermogravimetric balance, on an amorphous $\text{Co}_{20}\text{Ni}_{80}$ sample. The percentage change in mass is plotted as a function of increasing temperature. The early decrease in mass is due to the removal of adsorbed impurities. To check this, we performed an FTIR spectral study. We found that the as-prepared samples of Co–Ni contain strongly adsorbed CO

Table 1 Specific surface areas per unit mass of amorphous and heated samples of α -Co, γ -Ni, $\text{Co}_{20}\text{Ni}_{80}$, and $\text{Co}_{50}\text{Ni}_{50}$

sample	surface area/ $\text{m}^2\text{ g}^{-1}$		
	amorphous	heated at $300\text{ }^{\circ}\text{C}$	heated at $450\text{ }^{\circ}\text{C}$
α -Co	110	58	23
γ -Ni	76	55	25
$\text{Co}_{20}\text{Ni}_{80}$	150	50	34
$\text{Co}_{50}\text{Ni}_{50}$	135	43	30

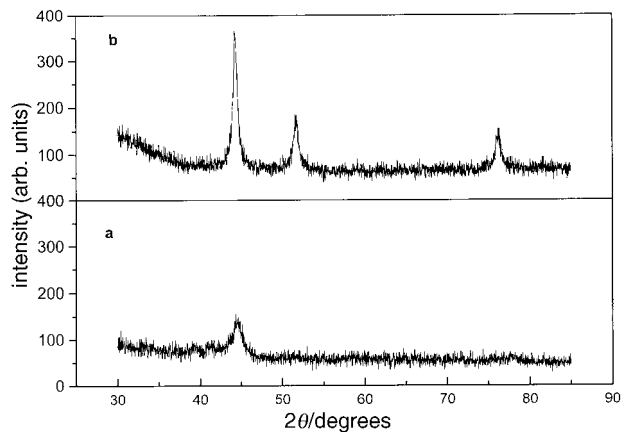


Fig. 7 XRD patterns for amorphous $\text{Co}_{20}\text{Ni}_{80}$ sample: (a) heat-treated at $300\text{ }^{\circ}\text{C}$ for 5 h, (b) heat-treated at $450\text{ }^{\circ}\text{C}$ for 5 h

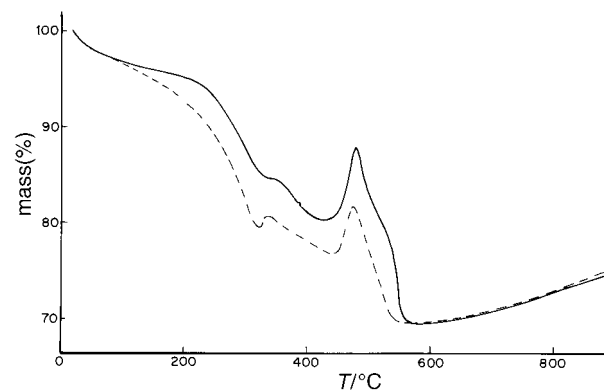


Fig. 8 Thermogravimetric measurements with a magnet on: (a) amorphous Co–Ni powder (solid line), (b) amorphous Fe–Ni powder (dashed line)

and hydrocarbon solvents on the surface. This is logical, since these nanostructured amorphous materials are highly porous, having a high surface area. The amorphous sample has a glass transition temperature (T_g) of $338\text{ }^{\circ}\text{C}$, and the Curie temperature (T_c) associated with the crystalline form of the alloy is observed at $565\text{ }^{\circ}\text{C}$. The behavior of the amorphous Co–Ni alloy system is very similar to the amorphous Fe–Ni reported earlier²⁹ [Fig. 8(b)].

The differential scanning calorimetric (DSC) curves of the as-prepared amorphous Co–Ni samples ($\text{Co}_{20}\text{Ni}_{80}$ and $\text{Co}_{50}\text{Ni}_{50}$) are shown in Fig. 9. Wide endothermic peaks below $300\text{ }^{\circ}\text{C}$, centered around 265 and $225\text{ }^{\circ}\text{C}$ for $\text{Co}_{20}\text{Ni}_{80}$ and $\text{Co}_{50}\text{Ni}_{50}$ samples respectively, are seen on these DSC curves.

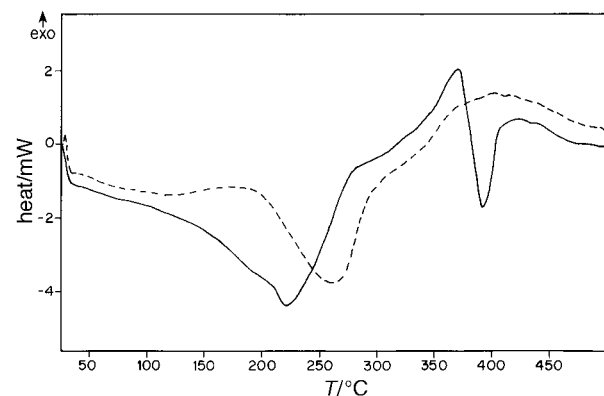


Fig. 9 Differential scanning calorimetric curves of the samples: (a) amorphous $\text{Co}_{20}\text{Ni}_{80}$ (dashed line), (b) amorphous $\text{Co}_{50}\text{Ni}_{50}$ (solid line)

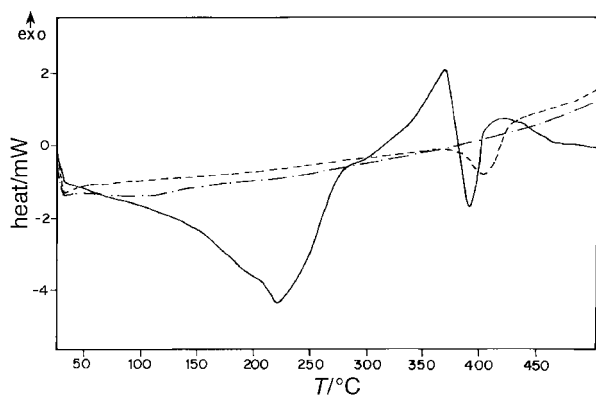


Fig. 10 Differential scanning calorimetric curves of amorphous $\text{Co}_{50}\text{Ni}_{50}$: (a) as prepared (solid line), (b) heat treated at 300°C for 10 h (dashed line), (c) the second run after cooling to room temperature (dot-dashed line)

Both these peaks disappear in the successive runs of the DSC and this indicates that they are desorption endotherms of the adsorbed surface impurities. The crystallization behavior of the two samples differs. The $\text{Co}_{20}\text{Ni}_{80}$ sample shows a wide exothermic peak centered around 400°C whereas the crystallization peak of the $\text{Co}_{50}\text{Ni}_{50}$ sample is a sharp one at 365°C . However, in this sample, the sharp exothermic peak is seen immediately followed by another sharp endothermic one. To check the possible role of the contaminants on this endotherm at 390°C , we have examined the DSC curve of a $\text{Co}_{50}\text{Ni}_{50}$ sample, after annealing at 300°C for 10 h to completely remove the surface adsorbed impurities. The endothermic peak is still seen on the DSC curve [see Fig. 10(b)], though shifted to 400°C . However, it is completely removed in the successive run [see Fig. 10(c)] showing the irreversible nature of the transition. From these observations, we believe that the second endotherm of the $\text{Co}_{50}\text{Ni}_{50}$ sample has to do with some kind of phase transition, the nature of which is not yet clear. Systematic and detailed studies, like thermomagnetometry (TM), and variable temperature XRD, are required.

Conclusions

Sonochemical decomposition of the solutions of volatile organic precursors, $\text{Co}(\text{NO})(\text{CO})_3$ and $\text{Ni}(\text{CO})_4$ in decalin at 273 K, under an argon pressure of 100 to 150 kPa (1 to 1.5 atm), yield amorphous, nanosized Co–Ni alloy particles. The composition of these alloy particles can be controlled by varying the initial precursor concentration in solution. Magnetic data indicate the superparamagnetic nature of the as-prepared amorphous sample and also the ultrafine nature of the crystallized sample.

This research was supported by Grant no. 94-00230 from the US–Israel Binational Science Foundation (BSF), Jerusalem, Israel. We thank the Ministry of Science and Arts, for the Binational Indo–Israel Grant. A. G. is grateful to the Bar-Ilan Research Authorities for supporting this project. R. P. acknowledges support from the Clore Foundations. We thank Prof. M. Deutsch for use of X-ray diffraction facilities and Prof. Y. Yeshurun for extending the facilities of the National Center

for Magnetic Measurements at the Department of Physics, Bar-Ilan University. We are grateful to Prof. S. Margel for the help in TG measurements, and to Dr. S. Hochberg for editorial assistance.

References

- 1 T. R. Anantharaman, *Trans. Tech.*, Aedermansorf, Switzerland, 1984.
- 2 P. Haasen and R. I. Jaffe, *Amorphous Metals and Semiconductors*, Pergamon, London, 1986.
- 3 N. F. Motte and E. A. Davis, *Electronic Processes in Non-Crystalline Materials*, Clarendon Press, Oxford, 1979.
- 4 H. Steeb and H. Warlimont, *Rapidly Quenched Metals*, Elsevier, Amsterdam, 1985.
- 5 T. Egami, *Rep. Prog. Phys.*, 1984, **47**, 1601.
- 6 F. E. Luborsky, in *Ferromagnetic Materials, Vol. 1*, ed. E. P. Wohlfarth, North-Holland, Amsterdam, 1980, p. 474.
- 7 C. A. Clark, *Br. J. Appl. Phys.*, 1956, **7**, 355.
- 8 C. Hitznerberger and H. P. Karnthaler, *Philos. Mag. A*, 1991, **64**, 151.
- 9 O. Blaschko, G. Krexner, J. Pleschiutchnig, G. Ernst, C. Hitznerberger, H. P. Karnthaler and A. Korner, *Phys. Rev. Lett.*, 1988, **60**, 2800.
- 10 J. M. Blanco, P. G. Barbon, A. R. Pierna and J. Gonzalez, *J. Non-Cryst. Solids*, 1991, **136**, 91.
- 11 A. Amamou, *IEEE Trans. Magn.*, 1976, **MAG-12**, 948.
- 12 E. M. Gyorgy, H. J. Leamy, R. C. Sherwood and H. S. Chen, *AIP Conf. Proc.*, 1976, **29**, 198.
- 13 M. Onoda, K. Shimizu, T. Tsuchiya and T. Watanabe, *J. Magn. Mater.*, 1993, **126**, 595.
- 14 M. Uzawa, A. Inoue and T. Masumoto, *Mater. Sci. Eng. A*, 1994, **181/182**, 1179.
- 15 G. Viau, F. Fievet-Vincent, F. Fievet, P. Toneguzzo, F. Ravel and O. Acher, *J. Appl. Phys.*, 1997, **81**, 2749.
- 16 K. S. Suslick, *Science*, 1990, **247**, 1439.
- 17 E. B. Flint and K. S. Suslick, *Science*, 1991, **253**, 1397.
- 18 A. A. Atchley and L. A. Crum, in *Ultrasound, its Chemical, Physical and Biological effect*, ed. K. S. Suslick, VCH, New York, 1988.
- 19 A. L. Greer, *Science*, 1995, **267**, 1947.
- 20 K. S. Suslick, D. A. Hammerton and R. E. Cline, Jr., *J. Am. Chem. Soc.*, 1986, **108**, 5641.
- 21 K. S. Suslick, S-B. Choe, A. A. Cichowlas and A. A. Grinstaff, *Nature (London)*, 1991, **353**, 414.
- 22 M. W. Grinstaff, M. B. Salmon and K. S. Suslick, *Phys. Rev. B*, 1993, **48**, 269.
- 23 R. Bellissent, G. Galli, T. Hyeon, S. Magazu, D. Majolino, P. Migliardo and K. S. Suslick, *Phys. Scr.*, 1995, **T57**, 79.
- 24 K. S. Suslick, T. Hyeon and M. Fang, *Chem. Mater.*, 1996, **8**, 2172.
- 25 Yu. Koltypin, G. Katabi, X. Cao, R. Prozorov and A. Gedanken, *J. Non-Cryst. Solids*, 1996, **201**, 159.
- 26 X. Cao, Yu. Koltypin, G. Kataby, R. Prozorov and A. Gedanken, *J. Mater. Res.*, 1995, **10**, 2952.
- 27 X. Cao, R. Prozorov, Yu. Koltypin, G. Kataby, I. Felner and A. Gedanken, *J. Mater. Res.*, 1997, **12**, 402.
- 28 K. V. P. M. Shafi, Y. Koltypin, A. Gedanken, R. Prozorov, J. Balogh, J. Lendvai and I. Felner, *J. Phys. Chem. B*, 1997, **101**, 6409.
- 29 K. V. P. M. Shafi, A. Gedanken, R. B. Goldfarb and I. Felner, *J. Appl. Phys.*, 1997, **81**, 6901.
- 30 *Binary alloy phase diagrams, Vol. 2*, American Society for Metals, Metals Park, Ohio, 1990, p. 145.
- 31 T. Pannaparayil, R. Marande, S. Komerneni and S. G. Sankar, *J. Appl. Phys.*, 1988, **64**, 5641.
- 32 X. Jiang, S. A. Stevenson, J. A. Dumesic, T. F. Kelly and R. J. Casper, *J. Phys. Chem.*, 1984, **88**, 6191.

Paper 7/06871I; Received 23rd September, 1997